Activation of Silicon Implanted with Phosphorus Atoms by Infrared Semiconductor Laser Annealing

Toshiyuki SAMESHIMA*, Masato MAKI, Megumu TAKIUCHI, Nobuyuki ANDOH,
Naoki SANO[1], Yasuhiro MATSUDA[2], and Yasunori ANDOH[2]

Tokyo University of Agriculture and Technology, Koganei, Tokyo 184-8588, Japan
[1]*Hightec Systems Corporation, Yokohama 222-0033, Japan*
[2]*Nissin Ion Equipment Co., Ltd., Koka, Shiga 528-0068, Japan*

We activated silicon implanted with phosphorus atoms by infrared semiconductor laser annealing with a diamond-like carbon (DLC) optical absorption layer. The silicon samples implanted with phosphorus atoms at 10 and 70 keV with concentrations of 5×10^{14}, 1×10^{15}, and 2×10^{15} cm^{-2} were coated with 200-nm-thick DLC films. The samples were annealed by irradiation with a 940 nm continuous wave laser at 70 kW/cm^2 with a beam diameter of 180 μm. The laser beam was scanned using a moving stage at 3–20 cm/s, which gave an effective dwell time of 0.9–6.0 ms. The amorphized surface regions were recrystallized by laser annealing longer than 1.2 ms. The in-depth profile of phosphorus concentration hardly changed within 5 nm for laser annealing for 2.6 ms. The sheet resistance markedly decreased to 106 and 46 Ω/sq for the samples implanted with phosphorus atoms at 10 and 70 keV by laser annealing at a dwell time of 2.6 ms, respectively. Phosphorus atoms were effectively activated with a carrier density near the phosphorus concentration for implantation at 70 keV. A low carrier generation rate was observed for implantation at 2×10^{15} cm^{-2} and 10 keV. An intermediate SiO$_2$ layer effectively blocked carbon incorporation to a level below 10^{17} cm^{-3}. [DOI: 10.1143/JJAP.46.6474]

KEYWORDS: DLC, mobility, carrier density, rapid annealing

1. Introduction

Rapid heating is important for activating semiconductor materials implanted with impurity atoms. A high activation ratio and no marked impurity diffusion are required to fabricate transistor devices. A method of flash lamp annealing for about 10 s and that of excimer laser annealing for about 10^{-9} s have been developed for this purpose.[1,2] We have also developed an annealing method on the order from 10^{-5} to 10^{-3} s using infrared lasers.[3,4] Infrared semiconductor lasers are an attractive light source because they can be high-power ~10 kW, high-efficiency ~50% and stable lasers. We use a carbon optical absorption layer in order to solve the problem of the low optical absorbance in infrared regions for silicon. Black carbon layers can have a high optical absorbance in an infrared rangion because of a high extinction coefficient and a low refractive index giving a low reflection loss. A black carbon layer with a high heat resistivity of ~5000 K can serve as a heat source at high temperatures.[5] Silicon is effectively heated by heat diffusion from the carbon layer placed adjacently.

In this paper, we report the annealing of silicon implanted with phosphorus atoms conducted using an infrared semiconductor laser. We demonstrate an effective activation and a low electrical resistance. We also report that initial phosphorus in-depth profiles are not significantly changed by laser annealing, and that the carrier density and carrier mobility can be analyzed on the basis of the free carrier optical absorption effect. We also discuss carbon contamination in silicon.

2. Experimental Procedure

The ion implantation of phosphorus atoms was conducted for p-type silicon substrates with a resistivity of 10 Ω cm. Acceleration energies were 10 and 70 keV. Concentrations
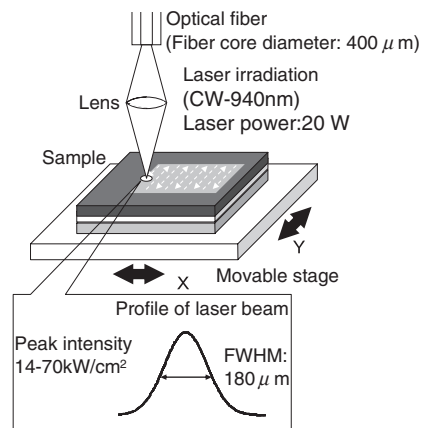

Fig. 1. Experimental setup for laser irradiation with CW semiconductor laser and beam scanning mechanism.

were 5×10^{14}, 1×10^{15}, and 2×10^{15} cm^{-2}. Graphitic-diamond-like-carbon (DLC) films with a thickness of 200 nm were formed on the silicon surface by unbalanced magnetron sputtering (UBMS) at room temperature with Ar gas at a radio frequency power of 30 W.[6] The deposition rate of the DLC films was 17 nm/min. Optical measurement revealed that the carbon layer had an optical absorbance of 70% at 940 nm, which was the wavelength of our laser light. Figure 1 shows the experimental setup for laser irradiation with a beam scanning mechanism. Samples were normally irradiated with a fiber-coupled continuous wave (CW) laser diode with a wavelength of 940 nm and a power of 20 W in air at room temperature. The diameter of the core and the numerical aperture (NA) of the fiber were 400 μm and 0.22, respectively. The diverged beam was concentrated on the sample surface using a combination of six aspherical lenses for 2 : 1 image formation. The power distribution of the beam was Gaussian like. The size of the beam spot was

*E-mail address: tsamesim@cc.tuat.ac.jp

180 μm at the full width at half maximum (FWHM) of the laser power distribution. The peak power density was 70 kW/cm^2 on the sample surface. Samples were mounted on an X–Y stage driven by linear motors in the constant velocity range from 3 to 20 cm/s in the Y-direction. The effective laser dwell time was given by the effective beam size of 180 μm divided by the laser beam scanning velocity. It ranged from 0.9 to 6.0 ms. The stage was also moved with a 50 μm step in the X-direction. After laser irradiation, the carbon layer was removed by oxygen plasma treatment. Numerical heat flow simulation was carried out to estimate temperature increase on the silicon surface.

Raman scattering spectral measurement using a 532 nm laser as an excitation light source was carried out in order to analyze crystalline states on the silicon surface. Using our microscopy system, we focused the laser light to a spot of 5 μm diameter on the surface and corrected back scattering light with a lens of 50 magnifications. This focus condition allowed the observation of crystalline states within the top 50 nm region in the depth direction. The phosphorus and carbon concentration in-depth profiles were measured by secondary ion mass spectroscopy (SIMS) analysis. The sheet resistance was also investigated using a four-point-probe measurement system. The free carrier absorption was analyzed to estimate the carrier concentration.[7,8]

In order to investigate an effect of blocking carbon incorporation from the carbon layer, we prepared p-type Si substrates coated with thermally grown 100-nm-thick SiO$_2$ layers. The Si samples were implanted with phosphorus atoms at 75 keV with a concentration of 2×10^{15} cm^{-2} via the SiO$_2$ layer. The peak concentration was positioned at the SiO$_2$/Si interface. SIMS measurement revealed that phosphorus atoms were effectively incorporated into Si at 1×10^{15} cm^{-2}, which was one-half of the total concentration. After the formation of the 200-nm-thick DLC layer on the surface of the SiO$_2$ layer, the samples were irradiated with the light of the CW laser diode at 940 nm and 70 kW/cm^2. The carbon in-depth profiles were measured by SIMS after removing the DLC layer. The sheet resistance was also measured after removing the SiO$_2$ layer.

3. Results and Discussion

In order to determine an appropriate laser annealing condition, recrystallization behavior was investigated for phosphorus implantation at 70 keV and with a concentration of 2×10^{15} cm^{-2}. The velocity of laser beam scanning from 20 to 3 cm/s resulted in the effective dwell time of the laser light from 0.9 to 6.0 ms. Figure 2 shows the Raman scattering spectra of the surface regions for the 2×10^{15} cm^{-2}-as-implanted and laser-annealed samples for each dwell time. The broad peak around 480 cm^{-1} for the as-implanted sample indicates that the silicon surface was almost completely amorphized by phosphorus ion implantation. The analysis of optical reflectivity spectra revealed that the 2×10^{15} cm^{-2} phosphorus ion implantation at 70 keV amorphized a top 150 nm region.[9] On the other hand, a sharp crystalline phonon peak was observed after laser annealing. This indicates that the surface region was recrystallized by laser annealing. Although a small and broad peak around 480 cm^{-1} still remained at the laser dwell time of 0.9 ms, a sharp crystalline phonon peak was only

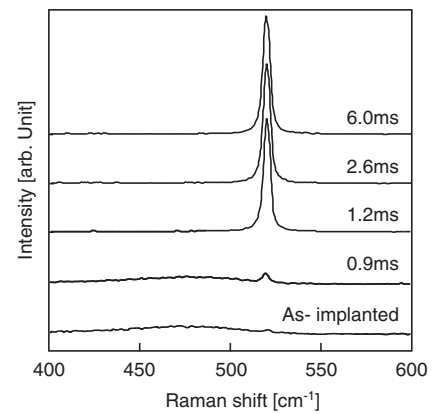Fig. 2. Raman scattering spectra of surface regions for samples 2×10^{15} cm^{-2}-as-implanted and laser annealed at various dwell times.

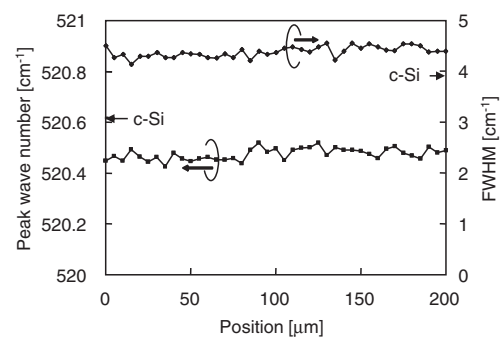Fig. 3. Distribution of peak wave number and band width of crystalline silicon phonon peak measured with 5 μm step for sample laser-annealed for 2.6 ms. The peak wave number and band width of bulk silicon are also represented by arrows.

observed at the laser dwell times of 1.2, 2.6, and 6.0 ms, as shown in Fig. 2. This indicates that the phosphorus-implanted surface regions were crystallized almost completely by laser annealing at 70 kW/cm^2 above 1.2 ms. By heat flow calculation, we estimated that the surface was heated to 1150 °C by laser irradiation for 0.9 ms. We also estimated that the temperature of the surface was increased to 1220 and 1390 °C by 1.2 and 2.6 ms laser irradiations, respectively. The result in Fig. 2 and the heat flow calculation indicate that the silicon surface was effectively crystallized in solid phase by heating to temperatures higher than 1200 °C. The spatial distribution of the Raman scattering spectra was measured in a 200-μm-long range with a step of 5 μm in the case of laser annealing for 2.6 ms using the moving stage for the Raman scattering measurement system as shown in Fig. 3. The measurement was conducted along the X-axis across the laser scanning direction shown in Fig. 1. The peak wave number and band width were almost the same for each measurement point over the 200-μm-long range, as shown in Fig. 3. This indicates that the silicon surface was uniformly annealed. The peak wave number was 520.46 cm^{-1}, which was slightly smaller than that of single crystalline silicon (520.62 cm^{-1}). The band width at FWHM was 4.4 cm^{-1}, which was slightly larger than that of single crystalline silicon (3.9 cm^{-1}). These differences in peak wave number and FWHM might be caused by internal stress due to phosphorus impurity doping.
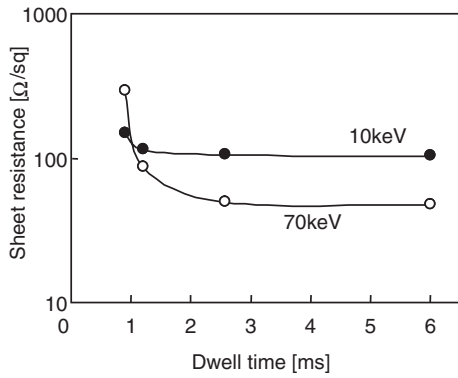
Fig. 4. Sheet resistance as a function of effective dwell time of laser light for 2×10^{15} cm^{-2} phosphorus implantations at 10 and 70 keV.

Figure 4 shows the sheet resistance as a function of the effective dwell time of laser light for phosphorus implantations at 10 and 70 keV with a concentration of 2×10^{15} cm^{-2}. The sheet resistance decreased to 106 and 46 Ω/sq for 10 and 70 keV at a dwell time of 2.6 ms. It almost leveled off at dwell times between 2.6 and 6.0 ms in both cases of 10 and 70 keV. On the basis of the results in Figs. 2–4, we assumed that phosphorus-implanted regions were well recrystallized and that phosphorus atoms were effectively activated at a laser dwell time of 2.6 ms. We therefore determined a dwell time of 2.6 ms given by a scanning velocity of 7 cm/s for further experiments.

Figure 5 shows the phosphorus atoms in-depth profiles of the samples 2×10^{15} cm^{-2}-as-implanted at 10 keV and laser-annealed (a), and as-implanted at 70 keV and laser annealed (b). The peak phosphorus concentration depths were 13.7 and 90 nm for the samples as-implanted at 10 and 70 keV, respectively. The phosphorus concentration gradually decreased to 1×10^{18} cm^{-3} as the depth increased to 77 nm for the sample as-implanted at 10 keV and to 246 nm for the sample as-implanted at 70 keV. No marked change in phosphorus concentration profile was observed after laser annealing at 70 kW/cm^2 for 2.6 ms, as shown in Fig. 5. After laser annealing, the peak phosphorus concentration was observed at 14.9 and 90 nm for the samples implanted at 10 and 70 keV, respectively. The depths at 1×10^{18} cm^{-3} were 80 nm for the sample as-implanted at 10 keV, and 247 nm for the sample as-implanted at 70 keV after laser annealing. The slight broadening of the depth profile of about 5 nm in the concentration range of 1×10^{20} to 4×10^{18} cm^{-3} was observed for the sample implanted at 10 keV after laser annealing. We consider that the silicon surface regions were heated to a very high temperature by laser annealing, causing the recrystallization of phosphorus-implanted regions. The diffusion coefficient of phosphorus atoms in solid silicon was about 1×10^{-11} cm^2/s at a very high temperature of around 1300 °C.[10] By heat flow calculation, we estimated that the heating duration for temperatures above 1300 °C was about 1.5 ms. The heating duration gives a diffusion length of 2.5 nm [$\sim 2 \times (1 \times 10^{-11} \times 1.5 \times 10^{-3})^{0.5}$], which is near our maximum diffusion length of 5 nm observed by SIMS, as shown in Fig. 5. Millisecond heat treatment will be important to activating the implanted regions while keeping initial dopant concentration profiles.
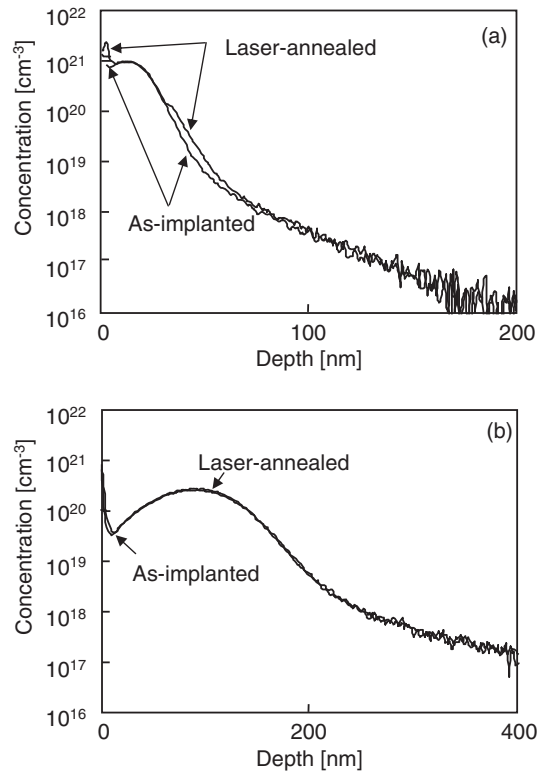

Fig. 5. Phosphorus atom in-depth profiles of samples implanted at 10 (a) and 70 keV (b) with a concentration of 2×10^{15} cm^{-2} measured by SIMS. Laser annealing was carried out at 70 kW/cm^2 for a dwell time of 2.6 ms.
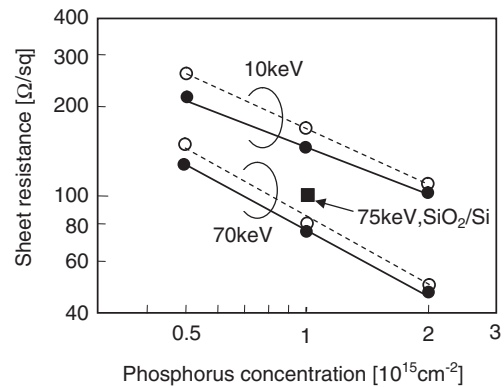

Fig. 6. Sheet resistance measured by four-point-probe method as a function of phosphorus concentration per unit area for implantations at 10 and 70 keV (solid circles and solid lines). Open circles and dashed lines represent the sheet resistances obtained by free carrier optical absorption analysis, as shown in Figs. 7 and 8. A solid square represents a sheet resistance obtained by the four-point-probe method for the 100-nm-SiO$_2$/Si sample implanted with phosphorus atoms at 75 keV with an effective concentration of 1×10^{15} cm^{-2}.

Solid circles and solid lines in Fig. 6 show the sheet resistance obtained using the four-point-probe measurement system as a function of phosphorus concentration per unit area. The sheet resistance markedly decreased to 46 Ω/sq as the phosphorus concentration increased to 2×10^{15} cm^{-2} for implantation at 70 keV. On the other hand, it only decreased to 106 Ω/sq for implantation at 10 keV. The results in Figs. 5 and 6 clearly show that the phosphorus atoms implanted in silicon were well activated by laser annealing

while almost keeping the initial in-depth profiles. The high resistance for implantation at 10 keV probably resulted from the marked impurity scattering effect due to a high phosphorus concentration of $\sim 6 \times 10^{20}\,\text{cm}^{-3}$, as shown in Fig. 6.

The electron free carrier optical absorption effect was analyzed in order to obtain the electron concentration and electron mobility. Optical reflectivity spectra were measured in the wave number range of 400 to 4000 cm^{-1} by conventional Fourier transform infrared (FTIR) spectrometry. The optical reflectivity spectra were analyzed using a numerical calculation program, which was constructed with the optical interference effect of an air/seven-layered doped Si/Si substrate structures. The optical reflectivity of the sample surface depends on the complex refractive indexes of Si, which consist of real refractive indexes and extinction coefficients. The free carrier in Si causes changes in real refractive index and extinction coefficient. These changes depend on the electron carrier density and carrier mobility. The thickness, carrier mobility and carrier density were changed for each of the seven doped layers for the calculation of the reflectivity. The light scattering effect caused by the roughness of the rear surface was also included in the program. The most possible in-depth distributions of the electron carrier density and carrier mobility were obtained by fitting the calculated reflectivity spectra to the experimental reflectivity spectra. The fitting process was conducted by a least-squares method. It gave an accuracy of a maximum carrier density within 15%.

Figure 7 shows the experimental reflectivity spectra for $2 \times 10^{15}\,\text{cm}^{-2}$ implantations at 10 and 70 keV, and the calculated spectra (a) and in-depth distributions of the carrier density (b) obtained by the fitting process shown in Fig. 7(a). The reflectivity spectra gradually increased as the wave number decreased. The change in the reflectivity of the sample implanted at 70 keV with wave number was larger than that at 10 keV. This is due to the typical optical interference effect observed when the peak carrier concentration region is buried deeply from the surface. The calculated spectra with carrier distributions shown in Fig. 7(b) were well fitted to the experimental spectra. The carrier was observed in only the surface region of the sample implanted at 10 keV. On the other hand, the peak carrier concentration was observed at 80–110 nm for phosphorus implantation at 70 keV. The in-depth carrier distributions had shapes similar to those of the phosphorus in-depth profiles, as shown in Fig. 5. Figure 8 shows the total carrier concentration (a) and minimum carrier mobility in the maximum carrier concentration region (b) as a function of phosphorus concentration per unit area. The total carrier concentration proportionally increased with phosphorus concentration for implantation at 70 keV. On the other hand, the rate of total carrier concentration increase decreased as the phosphorus concentration increased for implantation at 10 keV. This shows that a high phosphorus concentration has a low carrier generation probability. The minimum carrier mobility in the maximum carrier concentration region gradually decreased from 60 to 49 cm^2 V^{-1} s^{-1} for implantation at 70 keV and from 42 to 37 cm^2 V^{-1} s^{-1} for implantation at 10 keV as the phosphorus concentration increased. The decrease in minimum carrier mobility is due
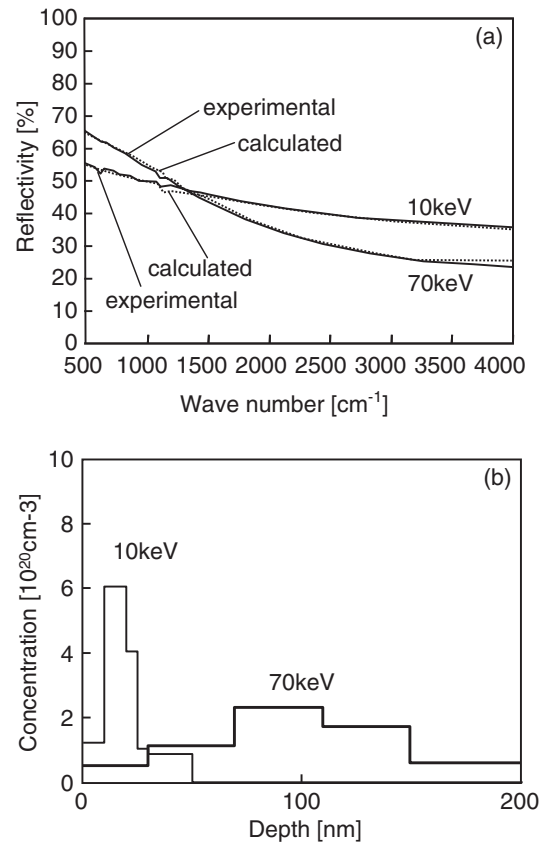

Fig. 7. Experimental optical reflectivity spectra in infrared region for $2 \times 10^{15}\,\text{cm}^{-2}$ implantations at 10 and 70 keV and spectra calculated using free carrier optical absorption effect (a) and carrier density in-depth distribution (b).

to the marked impurity scattering effect. The carrier mobility for implantation at 10 keV was lower than that for implantation at 70 keV. Phosphorus atoms concentrated in the surface shallow region for implantation at 10 keV, as shown in Fig. 5. This causes a high phosphorus volume concentration and induces a marked impurity scattering effect. Shallow doping inevitably results in a low carrier mobility. The sheet resistance was estimated using the carrier density and carrier mobility obtained by free carrier optical absorption analysis. It is given by the reciprocal value of the total conductance obtained by summing the conductances of all layers as,

$$R = \left(\sum_{i=1}^{7} e n_i \mu_i d_i \right)^{-1} \tag{1}$$

where R is the sheet resistance, e is the elemental charge, n_i is the carrier density at the ith layer, μ_i is the carrier mobility at the ith layer, and d_i is the thickness at the ith layer. Open circles and dashed lines in Fig. 6 show the sheet resistance estimated by free carrier optical absorption analysis. Although the sheet resistance obtained by free carrier optical absorption analysis was slightly higher than that measured by the four-point-probe method, we consider that the free carrier optical absorption analysis resulted in the carrier density in-depth profiles within the fitting accuracy on the basis of the results in Fig. 6.

Figure 9(a) shows the carbon in-depth profiles measured by SIMS for the sample as-implanted at 70 keV with $2 \times$
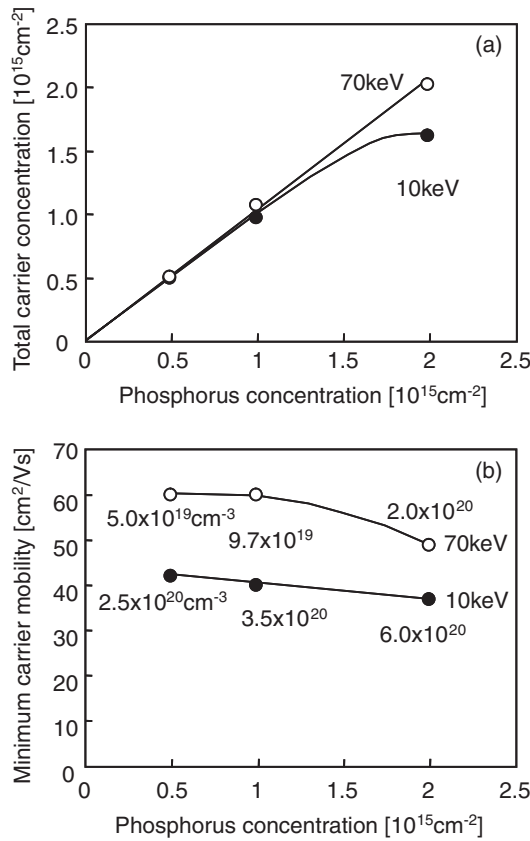
Fig. 8. Total carrier concentration (a) and minimum carrier mobility in maximum carrier concentration region (b) as a function of phosphorus concentration per unit area. The maximum carrier concentration is shown in (b).
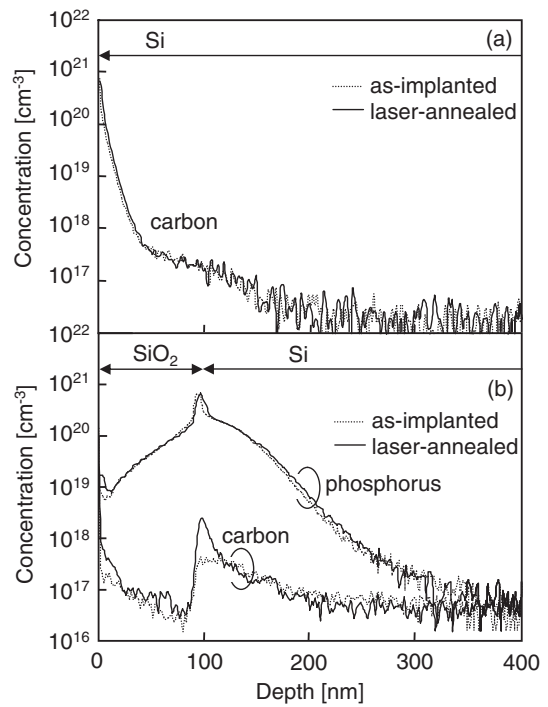

Fig. 9. Carbon concentration in-depth profiles for samples phosphorus-as-implanted at 70 keV with 2×10^{15} cm^{-2} into bare Si and laser-annealed at 70 kW/cm^2 for 2.6 ms (same sample shown in Fig. 5(b)) (a), and carbon and phosphorus concentration in-depth profiles for samples phosphorus-as-implanted at 75 keV with 2×10^{15} cm^{-2} into SiO$_2$(100 nm)/Si and laser-annealed at 70 kW/cm^2 for 2.6 ms (b).

10^{15} cm^{-2} phosphorus atoms and laser-annealed at 70 kW/cm^2 for a dwell time of 2.6 ms. A high carbon concentration of 9×10^{20} cm^{-3} was observed for the as-implanted surface, and a markedly high carbon concentration above 10^{18} cm^{-3} was observed at a depth of 25 nm from the surface, although no DLC layer was coated for the as-implanted sample for SIMS measurement. The laser-annealed sample with the DLC layer had a carbon in-depth profile similar to that of the as-implanted sample. This result indicates that the marked carbon contamination on the silicon surface caused difficulty in observing the behavior of carbon diffusion from the DLC layer into silicon. In order to obtain information on carbon diffusion and to achieve a silicon surface with a low carbon concentration, silicon samples coated with a thermal grown 100-nm-thick SiO$_2$ layer were used. As described in Experimental, 2×10^{15} cm^{-2} phosphorus atoms were implanted into silicon at 75 keV through the SiO$_2$ layer. Phosphorus atoms at a concentration of 1×10^{15} cm^{-2} were effectively implanted into silicon. The SIMS measurement of carbon profiles was carried out after implantation. Laser annealing at 70 kW/cm^2 for a dwell time of 2.6 ms was conducted after coating the SiO$_2$ layer with a 200-nm-thick DLC layer. The SIMS measurement of carbon profiles was also carried out after removing the DLC layer. Figure 9(b) shows the carbon and phosphorus in-depth profiles from the SiO$_2$ surface to the Si region including their interface. The carbon concentration was lower than 1×10^{18} cm^{-3} in SiO$_2$ deeper than 2 nm below the surface for the both samples

as-implanted and laser-annealed. This indicates that SiO$_2$ effectively prevented carbon incorporation. We believe that the carbon diffusion length in the SiO$_2$ layer was smaller than 2 nm during laser annealing. A thin intermediate SiO$_2$ layer effectively blocks carbon contamination. Most of the SiO$_2$ and Si regions had carbon concentrations below 10^{17} cm^{-3} except for the surface and interface regions. SIMS experts informed us that the high carbon concentration peaks observed at the SiO$_2$/Si interface resulted from extraordinary signals due to the discontinuous difference in ionization rate between SiO$_2$ and Si. Extraordinary peaks were also observed in phosphorus in-depth profiles, as shown in Fig. 9. The point measurement after removing the DLC and SiO$_2$ layers revealed that the sheet resistance decreased to 100 Ω/sq, as shown by a solid square in Fig. 6. This shows that the phosphorus atoms were activated to the same level of the samples without an SiO$_2$ intermediate layer.

4. Conclusions

A method of 940 nm CW laser annealing with a DLC optical absorption layer was applied to the activation of silicon implanted with phosphorus atoms. Phosphorus atoms were implanted to p-type silicon substrates at 10 and 70 keV with the concentration range of 5×10^{14} to 2×10^{15} cm^{-2}. DLC films with a thickness of 200 nm were formed on the silicon surface by a UBMS method. A laser beam of 180 μm diameter was used to irradiate samples at 70 kW/cm^2. When the dwell time of the laser beam was above 1.2 ms, the amorphized implanted region was almost completely re-crystallized. SIMS measurements revealed that the present

method of laser annealing at $70\,kW/cm^2$ and a laser dwell time of 2.6 ms hardly changed phosphorus concentration in-depth profiles within 5 nm. The sheet resistance markedly decreased to 102 and $46\,\Omega/sq$ for $2 \times 10^{15}\,cm^{-2}$ implantations at 10 and 70 keV after laser annealing, respectively. Free carrier absorption analysis gave a carrier concentration in-depth distribution similar to that of the as-implanted phosphorus concentration. The analysis also revealed carrier generation with a concentration similar to that of phosphorus atoms for implantation at 70 keV. On the other hand, a low carrier generation rate was observed for implantation at 10 keV and $2 \times 10^{15}\,cm^{-2}$. The carrier mobility decreased to 49 and $37\,cm^2\,V^{-1}\,s^{-1}$ as the phosphorus concentration increased for implantations at 70 and 10 keV. The carrier mobility for implantation at 70 keV was always higher than that for implantation at 10 keV. These resulted from a marked impurity scattering effect due to a high phosphorus concentration. The SiO_2 intermediate layer had an effective role in blocking carbon incorporation during laser annealing.

The carbon concentration was lower than $1 \times 10^{18}\,cm^{-3}$ 2 nm deep from the surface.

1) M. Mehrotra, J. C. Hu, and M. Rodder: IEDM Tech. Dig., 1999, p. 419.
2) K. Goto, T. Yamamoto, T. Kubo, M. Kase, Y. Wang, T. Lin, S. Talwar, and T. Sugii: IEDM Tech. Dig., 1999, p. 931.
3) T. Sameshima and N. Andoh: Jpn. J. Appl. Phys. **44** (2005) 7305.
4) N. Sano, M. Maki, N. Andoh, and T. Sameshima: AM-FPD Dig. Tech. Pap., 2006, p. 329.
5) T. Sameshima and N. Andoh: Mater. Res. Soc. Symp. Proc. **849** (2004) KK9.5.
6) S. Yamg, D. Camino, A. H. S. Jones, and D. G. Teer: Surf. Coat. Technol. **124** (2000) 110.
7) T. Sameshima, K. Saitoh, N. Aoyama, S. Higashi, M. Kondo, and A. Matsuda: Jpn. J. Appl. Phys. **38** (1999) 1892.
8) H. Engstrom: J. Appl. Phys. **51** (1980) 5245.
9) T. Sameshima, M. Takiuchi, M. Maki, N. Andoh, Y. Matsuda, Y. Andoh, and N. Sano: to be published in Proc. Workshop Active Matrix Flat Panel Displays and Devices.
10) A. S. Grove: *Physics and Technology of Semiconductor Devices* (Wiley, 1967) Chap. 3.